Towards characterising rhyolitic tephra layers from New Zealand with rapid, non-destructive μ-XRF core scanning

Peti, Leonie; Augustinus, Paul C.; Gadd, Patricia S.; Davies, Sarah

Published in:
Quaternary International

DOI:
10.1016/j.quaint.2018.06.039

Publication date:
2019

Citation for published version (APA):
Peti, L., Augustinus, P. C., Gadd, P. S., & Davies, S. (2019). Towards characterising rhyolitic tephra layers from New Zealand with rapid, non-destructive μ-XRF core scanning. *Quaternary International*, *514*, 161-172. https://doi.org/10.1016/j.quaint.2018.06.039

Accepted Manuscript

Towards characterising rhyolitic tephra layers from New Zealand with rapid, non-destructive μ-XRF core scanning

Leonie Peti, Paul C. Augustinus, Patricia S. Gadd, Sarah J. Davies

PII: S1040-6182(18)30252-0

DOI: 10.1016/j.quaint.2018.06.039

Reference: JQI 7499

To appear in: *Quaternary International*

Received Date: 4 March 2018

Revised Date: 19 May 2018

Accepted Date: 26 June 2018

Please cite this article as: Peti, L., Augustinus, P.C., Gadd, P.S., Davies, S.J., Towards characterising rhyolitic tephra layers from New Zealand with rapid, non-destructive μ-XRF core scanning, *Quaternary International* (2018), doi: 10.1016/j.quaint.2018.06.039.

Towards characterising rhyolitic tephra layers from New Zealand with rapid, non-destructive μ-XRF core scanning

Leonie Peti[1]*, Paul C. Augustinus[1], Patricia S. Gadd[2], Sarah J. Davies[3]

1 School of Environment, University of Auckland (New Zealand)

2 Australian Nuclear and Science Technology Organisation, Sydney (Australia)

3 Department of Geography and Earth Sciences, Aberystwyth University (Wales, UK)

* Corresponding Author: Leonie Peti, lpet986@aucklanduni.ac.nz; School of Environment, The University of Auckland, Private Bag 92019, Auckland 1142 New Zealand

Abstract

Tephra layers are of importance for the construction of reliable age control in late Quaternary paleoenvironmental and volcanic hazard studies, especially in volcanically-active settings such as the North Island of New Zealand. However, their identification involves time-consuming and destructive processing steps, making the application of non-destructive μ-XRF core scanners potentially advantageous for tephra identification. Here, we investigate the potential of the Itrax μ-XRF core scanner to differentiate between rhyolitic tephra layers sourced from various northern New Zealand rhyolitic volcanic centres deposited in maar lakes of the Auckland Volcanic Field. In their macroscopic form these tephra layers are usually visibly distinct when surrounded by a dark, organic-rich sediment matrix, although their attribution to source volcanic centre and eruption typically requires examination of their mineral assemblages, combined with chemical fingerprinting of the rhyolite glass shards. We demonstrate that μ-XRF core scanning of rhyolitic tephra layers from the Taupo Volcanic Zone and Tuhua Volcanic Centre can also allow identification, and sometimes differentiation, of the tephra using μ-XRF-derived elemental counts, especially high Si, K, Ca and very low Br and Ti. Different rhyolite tephra layers vary in their relative abundances of major, minor and trace elements as is evident from electron microprobe and LA-ICP-MS analyses of their glass shards. Mo-tube based μ-XRF cannot detect Na nor Mg and is of lower reliability for the lighter elements (Ca, Al) which play an important role in traditional tephra fingerprinting. Nevertheless, we are able to demonstrate that μ-XRF core scanning data can distinguish between previously identified tephra layers using multivariate statistics. Furthermore, the study emphasises the need for a standard protocol for μ-XRF core scanning of tephra layers for this approach to be more widely applicable,

especially to aid or be a substitute for conventional geochemical approaches used for tephra fingerprinting.

Keywords: Itrax; Tephra; Multivariate Statistics; Principal Component Analysis; Discriminant Factor Analysis; Auckland Volcanic Field, New Zealand

1 Introduction

Lake sediment-based reconstructions of late-Quaternary environmental change are only useful if based on reliable chronologies. Nevertheless, many of the changes in climatic and environmental conditions of interest occurred more than 50,000 years ago and/or cannot be dated by the radiocarbon technique. Fortunately, volcanic eruptions produce tephra that are deposited as layers both proximal and distal to volcanic centres and serve as time markers that aid the development of reliable chronologies (Shane, 2000; Lowe, 2011; Lane et al., 2017). This is the science of tephrochronology which is an important method for dating late Quaternary lake sediment sequences in northern New Zealand (Molloy et al., 2009).

Tephrochronology involves the unambiguous identification of tephra that are sometimes spread over large areas distal from the eruption site. Eruptions are effectively instantaneous events where they are preserved in the geological record so that the resulting tephra layers are isochrons. If the eruption has been dated by some means, the same age can be attributed to the widely-distributed tephra layers produced thereby underlining the importance of tephra to dating sediment-based records of past environmental change, as well as in volcanic hazard analysis (Shane, 2000; Lowe et al., 2008; Lowe, 2011).

To be able to establish reliable correlations between tephra layers encountered at different locations distal to the source and to proximal eruptive deposits, geochemical characterisation of the tephra is necessary and termed “fingerprinting”. Traditionally, tephra layers are fingerprinted geochemically and petrographically based on electron probe microanalysis (EPMA; for major element oxide composition), LA-ICP-MS (Laser ablation inductively coupled plasma mass spectrometry; for minor and trace elements) of volcanic glass and microscopic investigation of the diagnostic mineral assemblage (e.g., Shane, 2000; 2005; Shane and Smith, 2000; Lowe et al., 2008; 2013; Dugmore and Newton, 2012; Lane et al., 2017). However, this process is destructive and time consuming, thereby complicating the use of tephra as known-age isochrons in lake sediment sequences.

In contrast, µ-XRF scanning of sediment cores is fast, non-destructive and needs virtually no sample preparation (e.g., Croudace et al., 2006; Thomson et al., 2006; Croudace and Rothwell, 2010). Sediment-based records of past environmental change often routinely undergo µ-XRF scanning to obtain continuous time-series of geochemical data for elements with an atomic number Z ≥13 (Al to U). The geochemical data required for tephra recognition and identification/fingerprinting are collected automatically in the µ-XRF process. Hence, the potential advantages of being able to rapidly and reliably identify tephra using µ-XRF core scanners are clear.

Prior research into the potential of using µ-XRF core scanners as a tephrochronological aid has focussed on the ability to locate cryptotephra invisible to the un-aided eye (e.g., Balascio et al., 2015), or to identify tephra in lake sediment cores (Kylander et al., 2012). The latter authors do not recommend the use of µ-XRF core scanning data as a tool for tephra identification based on basaltic and low-concentration rhyolitic tephra layers in sediment cores from the Faroe Islands. However, improvements in the Itrax detector system and the abundance of macroscopic (visible) tephra layers with distinctive chemistries in New Zealand (Lowe et al., 2008) require a more thorough investigation of the potential of µ-XRF core scanning techniques for reliable tephra identification.

This study focuses on tephras in lake sediment cores retrieved from maars in the Auckland Volcanic Field (AVF; northern New Zealand) which unites outstanding high-resolution and finely-laminated records of late-Quaternary environmental change with well-preserved tephra deposits from a wide variety of volcanic systems (andesitic, basaltic, and rhyolitic).

2 The AVF

The AVF consists of about 53 basaltic volcanoes (Lindsay et al., 2011). Thirteen of these are explosion craters, called maars, formed by phreatomagmatic eruptions (Cas and Wright, 1988; Smith, 1989). All maar craters referred to in this study (Fig. 1) have hosted a lake for varying durations over the past ca. 250 ka (Molloy et a., 2009). Lake Pupuke is the only maar in the AVF which has not been in-filled and/or breached and contains an extant lake (Augustinus et al., 2006; 2008; Stephens et al., 2012; Newnham et al., 2018). The extant and in-filled maar lakes mostly have steep crater rims combined with deep lacustrine basins with small width to depth ratios resulting in excellent preservation potential of sediment and tephra derived from both tephra fall and reworking from the steep subaqueous crater rim slopes (Molloy et al., 2009; Zawalna-Geer et al., 2016).

The AVF maar lake sediment sequences often show pronounced fine laminations recording changes in regional climate and environmental conditions, possibly even at annual to decadal resolution

(Pepper et al., 2004; Augustinus et al., 2006; Striewski et al., 2013). For the past ca. 46 ka, good age control was largely established based on identification of geochemically-distinct, well-dated and well-preserved tephra (volcanic ash) isochrons (Shane, 2000; Molloy et al., 2009; Augustinus et al., 2011). This dependence on tephra layers for AVF maar lake sediment sequence chronology development highlights the need for fast and reliable identification of tephra in lake sediment cores proximal or distal to tephra-producing volcanic zones.

Figure 1 about here, over one column

2.1 Tephra records from the AVF maar crater lakes

The North Island volcanic centres (VC) that contribute rhyolitic and andesitic tephras to the Auckland maar lakes are located south of Auckland: the Okataina (OVC), Taupo (TVC), Egmont volcano (Eg; Taranaki) and Tongariro (TgVC) volcanic centres, as well as the smaller Tuhua VC (Mayor Island) to the SE. In addition, the c. 53 volcanoes in the AVF produced basaltic tephra which are dispersed locally (Fig. 1). Rhyolitic, basaltic and andesitic tephra from these centres have frequently reached the AVF maar lakes (Molloy et al., 2009; Zawalna-Geer et al., 2016), highlighting their value as known-age isochronous marker layers for both chronology development and correlation of the sediment sequences between maars. Furthermore, volcanic hazard assessment for the AVF basaltic volcanoes rely on identification of basaltic tephra layers contained in the maar lake sequences although their timing has largely been constrained by the bracketing known age rhyolitic tephra (Molloy et al., 2009; Hopkins et al., 2015). However, new approaches using $^{40}Ar/^{39}Ar$ dating of the basaltic lava flows from the source AVF volcanoes correlated to basaltic tephra deposits (Hopkins et al., 2017; Leonard et al., 2017), zircon double-dating (Danišík et al., 2012), and meteoric ^{10}Be and magnetic paleointensity studies of the maar lake sediments (Nilsson et al., 2011) have the ability to dramatically improve the chronology of the sequences beyond the ^{14}C-dating- method limit of c. 60 cal ka under favourable conditions.

In this study, we investigate the scanning μ-XRF characteristics of rhyolite tephra layers in sediment cores from five AVF maar paleolakes: Onepoto Domain, Orakei Basin, Panmure Basin, Hopua Crater, and Pukaki Lagoon; plus one extant lake, Pupuke (Fig. 1). Only rhyolite tephra layers were used as they are the most widely-dispersed and widely-used tephrochronological deposits in New Zealand.

3 Material and methods

3.1 Rhyolitic tephra layers

126 The tephra records documented in sediment cores from Hopua maar, Lake Pupuke and the Orakei
127 Basin core collected in 2007, Pukaki and Onepoto maars are presented in Table 1. Figures 2 and 3 in
128 Molloy et al. (2009) present the studied rhyolitic tephra layers in stratigraphic context of the
129 Auckland Volcanic Field maar lake records. This study focusses only on macroscopic rhyolitic tephra
130 layers which have previously been identified through EPMA glass chemical composition (Molloy et
131 al., 2009 and unpublished data by Zawalna-Geer). Table 1 summarises the names, source volcanic
132 centres and dominant mineralogy of the 13 rhyolitic tephra layers investigated in this study.

133

134 Table 1: Overview over investigated rhyolitic tephra layers in this study following Lowe et al. (2008)
135 and Molloy et al. (2009).

Name	Ferromagnesian mineralogy[2]	Centre[1]
Tuhua	aeg > cpx > opx ± aen ± rie ± hb ± olv(fa) ± tuh	TUVC
Mamaku	hb > opx >> ± cgt	OVC
Rotoma	cgt > hb	OVC
Opepe	opx >> cpx	TVC
Waiohau	opx > hb	OVC
Rotorua	bio > opx > hb	OVC
Okareka	bio	OVC
Kawakawa/Oruanui	opx > hb	TVC
Okaia	opx > hb	TVC
Hauparu	hb, opx	OVC
Maketu	hb > opx	OVC
Tahuna	opx > hb	TVC
Rotoehu	bio = hb = cgt	OVC

136 [1]TUVC: Tuhua Volcanic Centre (Mayor Island); OVC: Okataina Volcanic Centre; TVC: Taupo Volcanic
137 Centre

138 2 aeg: aegirine; aen: aenigmatite; bio: biotite; cgt: cummingtonite; cpx: clinopyroxene; hb:
139 hornblende; olv(fa): olivine (fayalite); opx: orthopyroxene; tuh: tuhualite. ± indicates may or may not
140 be present.

141 3.2 Methods

142 3.2.1 µ -XRF Core Scanning

The sediment cores were scanned with three different Itrax µ-XRF Core Scanners (Cox Analytical Systems, Gothenburg, Sweden) at Aberystwyth University (AU, UK), the Australian Nuclear and Science Technology Organisation (ANSTO, Australia), and The University of Auckland (UOA, New Zealand) with settings specified in Table 2. Each scan resulted in an optical image, a radiograph and single dispersive energy spectra for each interval measured along the core profile. Integrated peak area integrals for each element are calculated from the spectra which are then output as X-ray fluorescence (XRF) count data (Croudace et al., 2006; Thomson et al., 2006; Croudace and Rothwell, 2010).

Table 2: Overview of µ-XRF scanning locations and conditions used in this study

Site	Location of scan	Year of scan	X-ray tube	Voltage	Current	XRF exposure time	Step size
Pupuke	AU[1]	2008	Mo	30 kV	20 mA	10 s	200 µm
Hopua	AU	2008	Mo	30 kV	45 mA	10 s	200 µm
Panmure	AU	2010	Mo	30 kV	45 mA	10 s	200 µm
Onepoto	ANSTO[2]	2013	Mo	30 to 55 kV	50 to 55 mA	10 s	1000 µm
Orakei	UOA[3]	2017	Mo	30 kV	55 mA	10 s	1000 µm
Hopua	UOA	2017	Mo	30 kV	55 mA	10 s	1000 µm
Panmure	UOA	2017	Mo	30 kV	55 mA	10 s	1000 µm
Onepoto	UOA	2017	Mo	30 kV	55 mA	10 s	1000 µm

[1]: Aberystwyth University; [2]: Australian Nuclear Science and Technology Organisation; [3]: University of Auckland

3.2.2 Data Treatment

To correct for variability in sediment water, organic matter content and grain size, as well as X-ray tube ageing, all elemental peak intensities have been normalised to the sum of incoherent and coherent scattering (inc+coh; Löwemark et al., 2011; Kylander et al., 2012). Unless otherwise stated, element "X" refers to elemental peak areas normalised by inc+coh (Fig. 2).

Figure 2 about here, landscape over full page

As an initial step, we examined the kernel density estimation (KDE) of the distribution of elemental counts of Al, Si, P, S, Cl, K, Ca, Ti, V, Mn, Fe, Ni, Zi, Br, Rb, Sr, Zr (all normalised to inc+coh) and inc+coh (Fig. 3, 4). KDE estimates the probability density function of the variable in question and can be understood as a smoothed version of a histogram.

Most elements follow approximately log-normal distributions. Some elements display bimodal distributions within the general shape of a log-normal distribution (Fig. 3). The bimodality was largely preserved after log-ratio transformation with many elements showing skewed distributions to various degrees (Fig. 3, 4). A condition of the statistical tests described below is normal distribution of the data (Zelterman, 2015). To obtain roughly normally distributed data the normalised counts have been log-ratio transformed.

The bimodality and skewed distributions (Fig. 3) partly result from mixing µ-XRF scanning data from different Itrax scanners using different detector generations (Fig. 4, Table 2). The maximum counts a new detector (i.e., the Itrax at the University of Auckland) can record are several times higher than those of the older detector (i.e., the Itrax at the Aberystwyth University in 2008). Despite normalizing the data by inc+coh, substantial differences in the numerical counts remain (Fig. 4). These differences between detectors have a stronger influence on the distribution shape than actual differences in element "X" between the tephra layers, thereby causing a skewed or multimodal shape. K_{norm}, Ca_{norm} and Sr_{norm} are presented in Fig. 4 as an example separated by tephra layer (colour) and Itrax scanner (line pattern). Although differences between the tephra layers can generally be observed, differences between the Itrax scanners become apparent too. For example, the distribution of the Tahuna tephra reaches its respective peaks of K_{norm} (Fig. 4) in the lower end of the entire distribution in the µ-XRF data from ANSTO and in the middle part in the data from UOA. However, the Mamaku tephra is consistently recorded with overlapping highest density of the Ca_{norm} and Sr_{norm} distribution in µ-XRF data from UOA and AU. Additionally, it becomes clear that different tephra layers show distinct peaks in the density distribution of normalised µ-XRF counts, thus pointing to the possibility of geochemical differentiation between tephra layers based on µ-XRF counts.

For further analyses, the tephra layers have been split into pre-Kawakawa/Oruanui tephra (KOT, inclusive) layers and post-KOT layers. The KOT is the product of a caldera-forming super eruption 25,360 ± 160 cal yr BP (Pillans et al., 1993; Vandergoes et al., 2013) that produced widely-dispersed tephra.

194 Data from three different Itrax µ-XRF core scanners

195 Mixing µ-XRF scanning data from different Itrax scanners used with different detector generations
196 and different scanning settings cause complications for numerical analyses which cannot be
197 corrected for easily. Hence, we split the dataset by core scanner location and only proceed with data
198 from the ANSTO Itrax (for pre-KOT) and the UOA Itrax (for post-KOT), separately for further
199 multivariate statistical analyses. The decision to exclude the data from the AU Itrax was motivated
200 by the smaller number of scanned tephra layers, the older detector[1] used with lower sensitivity for
201 lighter elements and different scanning settings from the ANSTO and UOA Itrax scans (see Table 1).

202 The logarithm of "0" is not defined. Hence, special care must be taken when applying log-
203 transformation to data including "0". Only elements which have been measured in all scanning
204 routines are kept for interpretation to avoid introducing artificial 0-values. Additionally,
205 measurements of some elements of low abundance and/or low detection limit in the µ-XRF
206 technique (e.g., Al) result in "0" in many measurements. Cuven et al. (2007) recommended
207 removing all elements that include more than 30% of 0-values. All measurements that still include
208 one or more 0-values after this step must also be removed, resulting in the possible removal of the
209 thinner tephra layers that are represented by fewer µ-XRF data points. Hence, we chose to remove
210 all elements that include more than 10% of 0-values and remove the few remaining measurements
211 including 0-values.

212 *Figure 3 about here, landscape over full page*

213 *Figure 4 about here, landscape over full page*

214

215 Data transformation

216 Elemental counts obtained from µ-XRF scanning are compositional data consisting of proportions
217 summing to a constant and are non-negative (Aitchison, 1986). Hence, the variation of one
218 component of the total (i.e., an element "X" whether it can be detected by the Itrax or not)
219 influences the amount of all other elements. This unit-sum constraint possibly results in incorrect
220 inference when improperly incorporated into the statistical analyses and is well known in the
221 geostatistical community (e.g., Lowe et al., 2017). Aitchison (1986) has developed a simple approach
222 to removing this constraint by applying log-ratio transformation where the natural logarithm of
223 ratios between two components of the sum are computed. Note, however, that all the data

[1] Note that the Aberystwyth University Itrax detector has been upgraded in 2008 and 2015 with improved sensitivity.

presented here are ratios because they have been normalized by inc+coh. Many authors favour log-ratio transformation (e.g., Weltje and Tjallingii, 2008; Weltje et al., 2015; Martin-Puertas et al., 2017) whereas others question its use (e.g., Pearce et al., 2008; Feng et al., 2014). Lowe et al. (2017) point out that any statistical analyses should ideally be performed on transformed and un-transformed data and if transformation alters the results obtained caution has to be taken with the use of the dataset. Hence, all the following statistical approaches applied to the rhyolite tephra µ-XRF data involve log-ratio transformed and raw (normalised) data to compare results. The results of both approaches are very similar giving confidence to the presented µ-XRF-based geochemical fingerprinting approach.

Principal component analysis

Principal component analysis (PCA) finds the direction of highest variance within the multivariate data and fits the first principal component (PC) along this direction. Each subsequent component describes a subsequently smaller amount of variance of the original dataset and is oriented orthogonally to the prior component (e.g., Zelterman, 2015). In the resulting biplot, the proximity of the data points to each other suggests a strong similarity between the measurements, while proximity between the elemental loadings and data points emphasises the correlation between the respective type of material (sediment or certain tephra layer) and the measured elements (e.g., Zelterman, 2015).

PCA has been applied to µ-XRF scanning results from the Onepoto core measured at ANSTO (Fig. 7A), µ-scanning results from the Hopua core measured at the University of Auckland (Fig. 7B), pre-KOT rhyolitic tephra layers in the Onepoto core (measured at ANSTO (Fig. 7A), and post-KOT rhyolitic tephra layers in the Hopua and Panmure cores (measured at University of Auckland) (Fig. 7B).

Discriminant function analysis

Linear discriminant analysis (LDA) is a subclass among discriminant function analyses that determines a linear combination of independent variables (here elemental intensities) leading to a single transformed variable by which *a-priori* classified, mutually exclusive groups (here tephra layers classified by EPMA data) may be discriminated (e.g., Zelterman, 2015). The first linear discriminant function (LD) achieves the largest separation between the pre-classified groups similar to the 1st PC. LDA has been successfully applied to EPMA data of tephra layers in New Zealand to discriminate between previously classified tephra layers and test the applicability to identify

subsequently encountered tephra layers (Stokes and Lowe, 1988; Stokes et al., 1992; Shane and Froggatt, 1994; Cronin et al., 1996).

4 Results and Discussion

4.1 Geochemical distinction between rhyolitic tephra layers and sediment matrix

Variability in elemental counts obtained by µ-XRF scanning clearly shows the rhyolitic tephra layers in sediment cores (Fig. 4), which works well when the intervening sediment is organic matter-rich resulting in marked geochemical contrast between lake sediment and tephra layers. Thinner tephra layers are more difficult to locate by µ-XRF scanning than thicker tephra layers. Practically, there is no clear minimum thickness for a tephra layer in order to be located and identified by this technique. If a strong contrast in chemical composition to other tephra layers exists even <200 µm tephra layers may be identified by this technique in the future. However, for statistical reliability a minimum thickness of c. 1 mm is favourable for this technique.

PCA of normalised elemental counts highlights the power to differentiate between lacustrine/marine sediment and rhyolitic tephra layers based on µ-XRF core scanning data (Fig. 5).

During µ-XRF scanning, Si, K and Ca are consistently elevated in the rhyolitic tephras with respect to the sediment matrix. The high counts of the latter elements are consistent with the geochemistry of the rhyolitic tephra (Winter, 2001; Lowe et al., 2008). Furthermore, most rhyolitic tephra layers are positively correlated to Mn, Rb and Sr as identified by PCA (Fig. 5). In contrast, rhyolitic tephra layers are always relatively depleted in Br which is consistent with Br being an indicator for organic rich sediment (Davies et al., 2015; Rothwell and Croudace, 2015; note the correlation of Br with lacustrine sediment in all PCA results in Fig. 5). It is striking that Zn, Rb, Sr and Zr vary in their behaviour between discrete tephra layers of different ages, e.g., Zr is high in the Maketu, Hauparu and Tuhua layers compared to the amounts in the encapsulating sediment whereas Sr is elevated in most tephra layers but depleted in the Tuhua layer (Fig. 4).

The µ-XRF presented data shows that tephra layers sourced from the TVC are chemically distinct from those sourced from the OVC and from those erupted by the TUVC as has been observed in conventional tephrochronological methods (e.g., Lowe et al., 2017). This finding provides confidence that µ-XRF core scanners have the potential to fingerprint rhyolitic tephra layers to their source volcanic centre.

Figure 5 about here, landscape over full page

287

288 4.2 Multivariate geochemical discrimination between the rhyolitic tephra layers

289 Most discrete rhyolitic tephra layers such as the Rotoehu, Tahuna, Maketu, Hauparu, Okaia,
290 Okareka, Waiohau, Rotoma and Tuhua tephra are strongly depleted in Ti whereas the
291 Kawakawa/Oruanui (KOT) and Rotorua tephra show no discernible difference in levels of Ti
292 compared with that of the sediment matrix. Only the Mamaku and Tuhua tephra are enriched in Fe
293 (Fig. 2B). Tahuna, Maketu, Hauparu and Tuhua tephra are enriched in Zn compared to the amounts
294 in the sediment matrix and the rhyolite tephra layers, except for Okareka and Mamaku tephra, are
295 enriched in Rb (Fig. 2). Tuhua is the only tephra clearly depleted in Sr while all other rhyolitic tephra
296 layers examined are enriched in Sr to various degrees. The Maketu, Hauparu, KOT, Rotorua,
297 Waiohau and Tuhua tephra layers are strongly enriched in Zr. All the other tephra layers show no or
298 very minor differences in Zr levels between the sediment and the tephra (Fig. 2).

299 Comparing only the tephra layers to one another indicates that the different layers form different
300 clusters in a biplot (Fig. 6) and linear discriminant analysis (Fig. 7). The thin tephra layers (Okaia,
301 Hauparu, Tahuna, Mamaku, Opepe and Waiohau) are not easily identifiable due to the limited
302 number of data points available due to their thickness. High-resolution (200 µm) µ-XRF scans over
303 multiple lateral positions of thin tephra layers may increase the possibility of identifying the thick
304 tephra layers.

305 Pre-KOT rhyolite tephra

306 PCA and LDA enabled identification of the largest difference between Rotoehu and the four other
307 pre-KOT rhyolitic tephra layers (Fig. 6A, 7A). Separation along PC1 and LD1 is mostly achieved with
308 Rotoehu tephra which is relatively enriched in Si, Sr, K and Rb, whilst displaying relative depletion in
309 Ca, Zn, Fe, Cl and Mn. PC2 and LD2 achieve a clear separation between the Maketu/Hauparu and
310 Tahuna/Okaia tephra, respectively, with the former being relatively enriched in Ca, Rb, Si, Ti and Fe
311 and the latter relatively enriched in Mn, Sr and K (Fig. 6A, 7A). Along LD2, the Maketu, Hauparu and
312 Rotoehu tephra form one cluster (Fig. 6A, 7A) corresponding to the OVC-source of these three
313 tephra layers (Table 1, Fig. 1). The other cluster along LD2 is formed by Okaia and Tahuna tephra and
314 corresponds to their TVC source (Fig. 1, 7A). Fig. 6A shows scattered outliers, especially in the lower
315 left corner where Tahuna and Okaia tephra chemistries mix (Fig. 7A). The observed wide scatter of
316 data points emphasizes the need for more elemental data points, especially for the thinner tephra
317 layers to better constrain the tephra-source defined clusters and remove outliers.

318 Post-KOT rhyolite tephra

PCA and LDA plots show clear elemental differentiation between the Tuhua and all other post-KOT tephra (Fig. 2B, 5B) which is consistent with it being the only tephra from the Tuhua Volcanic Centre examined in this study and its contrasting composition to the others as noted in earlier studies based on glass shard EPMA data (e.g., Lowe et al., 2008). Tuhua tephra is relatively enriched in Fe, Zn, Zr, Y, and Mn and depleted in Sr (Fig. 2B). Hence, PC1 and LD1 allow separation of the Mayor Island-sourced tephra from the remaining post-KOT rhyolitic tephra layers. Rotoma, Rotorua and Opepe tephra each have sufficient data points to produce well-defined clusters in the PCA bi-plot (Fig. 2B). PC2 largely allows elemental discrimination between Rotorua (relatively enriched in Ca) and Opepe tephra (Fig. 2B). The same trend is visible, but clearer, in the LDA where LD3 achieves separation between TVC and OVC+TU sourced rhyolitic post-KOT tephra layers (Fig. 5B).

Figure 6 about here, landscape over full page

Figure 7 about here, one and a half page width

4.3 Bivariate scatterplots

Using multivariate statistics, a suite of bivariate scatterplots showing the clearest separation of individual tephra layers can be produced and is supplemented by typical bivariate scatterplots for rhyolitic tephra (e.g., SiO_2 vs. K_2O; Shane, 2000) identification based on traditional EPMA data in Fig. 8.

Pre-KOT rhyolite tephra

All pre-KOT elemental scatterplots (Fig. 8A) show the outliers of the Rotoehu, Maketu, Hauparu and Okaia tephra layers at a significant distance from their respective clusters as was observed in the PCA biplots (Fig. 6A). A standard bivariate plot used by the tephrochronological community for differentiating between and fingerprinting tephra layers to source, and possibly event of an eruption, is SiO_2 vs. K_2O (e.g., Shane, 2000). However, the equivalent µ-XRF scanning of Si vs. K plot of log-transformed µ-XRF core scanning data only achieves clear separation between Okaia+Tahuna vs. Rotoehu+Maketu+Hauparu tephra (Fig. 8A). Bivariate plots of Ca vs. K, Fe vs. Ca, Si vs. Zn, Sr vs. Ca and Rb vs. Sr (Fig. 8A) show a clear separation between the Maketu and Rotoehu tephra. The lower number of µ-XRF data points for the Okaia and Tahuna tephra as well as the large variance in µ-XRF elemental counts complicate the recognition of a clear cluster corresponding to their mean

count values of the latter elements. It is not possible to conclude whether the data points distal from the centre of the cluster are outliers due to scanning or core condition (e.g., small amounts of foreign material mixed with the tephra layer not visible at the core surface) or if these tephra layers exhibit a large variance in the elements possibly due to pre-, syn- and/or post-eruptive processes.

Using this µ-XRF scanning approach has not enabled clear geochemical separation between the Okaia and Tahuna tephra, nor separation of the Hauparu from the Maketu tephra (Fig. 8A). This further highlights the need for more elemental data points from each of the tephra layers, particularly the thinner layers (Fig. 2) to be able to better define mean count values of the elements, their variance, and hence, delineate possible outliers. In addition to acquiring more elemental data points during the scans, future work requires investigation of a greater range of elements, especially minor and trace elements[2], which could achieve a clearer geochemical separation of the visually-distinct tephra.

Post-KOT Rhyolite Tephra

Scatterplots of Si vs. K, Ca vs. K, Fe vs. Si, Mn vs, Si, Ti vs. Cl, and Y vs. Cr for post-KOT rhyolitic tephra layers shown in Fig. 8B highlight the ease of differentiation of the Tuhua tephra from all others examined here. The thicker Rotoma and Rotorua layers can also be separated clearly despite an abundance of outliers, especially in the more common EPMA-based geochemical bivariate plots used commonly in tephrochronology (e.g., SiO_2 vs. K_2O, CaO vs. K_2O, Fe_2O_3 vs. SiO_2; Shane, 2000). The nature of these outliers is unclear but more precise Ca and Si µ-XRF elemental data and potentially fewer outliers could be achieved on the Itrax µ-XRF core scanner using the Cr-tube as it has lower detection limits for light elements. The minor elements contribute to separation of the post-KOT tephra layers with fewer outliers evident in Mn vs. Si, Ti vs. Cl and Y vs. Cr bivariate plots (Fig. 8B). The Opepe and Waiohau tephra do not plot as clearly defined clusters although the Opepe tephra data points define a zone where most of its elemental data points lie.

Figure 8 about here, landscape over full page

5 Conclusions

This study demonstrates the potential of rapid and non-destructive µ-XRF core scanning for separating rhyolitic tephra layers sourced from different volcanic centres, and sometimes different eruptives from the same centre using elemental composition. The ability to use compositional

[2] Following definition by glass shard geochemistry: major elements expressed as oxides are usually defined as>1 wt %, minor element oxides as 0.1 to 1 wt %, and trace elements as<0.1 wt % or <1000 parts per million (ppm) of the element (Lowe et al., 2017).

379 analyses derived from μ-XRF core scanning as an aid to tephrochronology is abetted by the organic-
380 rich lacustrine sediment interbedded with the tephra infilling the Auckland maar lakes that allow
381 clear differentiation of the rhyolite tephra. This was able to be achieved despite the μ-XRF core
382 scanner measurements being generated using a Mo tube so that the light element data (Al, Ca) were
383 of lower precision than if a Cr tube was used. These elements are typically useful in conventional
384 tephra fingerprinting using major oxide data derived from electron microprobe analysis. Analyses of
385 minor and trace elements can be useful in tephra fingerprinting (e.g. Pearce et al., 2007; Davies et
386 al., 2012; Wastegård et al., 2013; Lowe et al., 2017), which are easily and quickly obtained by μ-XRF
387 core scanning during the same analysis as major elements are acquired. Consequently, future
388 studies should evaluate the full potential of the μ-XRF scanning technique for tephra fingerprinting
389 by varying the scanning settings and elements used. In particular, exposure time per measurement
390 interval and scanning settings need to be adjusted in order for the elemental counts to exceed "0"
391 where relevant, in order to avoid discarding many minor and trace elements that may be of
392 significance. Only then can the whole range of geochemical variability between tephra layers be
393 captured and utilised. Similarly, obtaining Al and Ca counts as high as possible might need to be the
394 focus when choosing the X-ray tube (favouring the Cr-tube for the light elements) and adjusting
395 scanning settings (kV, mA) and exposure time accordingly.

396 This study also shows that many factors, such as current (mA), voltage (kV) and exposure time
397 influence scanning results in a non-linear manner. Their influence has not yet been quantified and
398 we propose to avoid these complications by following a standard protocol for tephra
399 characterisation. Experimental scans of tephra layers to be undertaken in the future should
400 determine ideal current, voltage and exposure time to enable robust data comparison and
401 application of multivariate statistics.

402 An additional complication for robust tephra μ-XRF based fingerprinting arises from the difference
403 between different generation detector systems and related settings in the Itrax μ-XRF core scanners
404 used in this study. Despite normalisation of elemental count data, significant differences between
405 data sets from the same maar cores and tephra layers scanned by different core scanners remained.
406 To avoid this complication in the future, we propose to conduct all further tephra μ-XRF scans for
407 New Zealand tephra layers on the same Itrax core scanner following a standard protocol.

408 The results of the present study suggest that only one or two bivariate scatterplots (e.g., Ca vs. K, Rb
409 vs. Sr, Y vs. Cr; Fig. 8) of μ-XRF core scanning data may be enough to fingerprint one or more rhyolite
410 tephra layers. However, thin tephra layers, such as the Tahuna, Hauparu, Okaia, Okareka, Waiohau,

411 Opepe and Mamaku examined in the present study need to be investigated with repetitive μ-XRF
412 scans to obtain greater data density for the statistical approaches used.

413 Using these protocols, it is possible to establish a database of many μ-XRF scanning results from
414 tephra layers already identified using EPMA-based approaches which can be used as the input to
415 semi-automated machine learning algorithms to reliably identify rhyolitic tephra and thereby
416 decrease the time involved in tephra fingerprinting for tephrochronology in a non-destructive
417 manner. To be able to utilize this method of μ-XRF core scanning-based tephra fingerprinting to its
418 full potential, the approach will need to be extended to basaltic and andesitic tephra layers that are
419 commonly encountered in the AVF maar lakes sediment cores. Subsequently, tephrochronologists
420 working in other regions of the globe in which tephra layers of sufficient thickness are found in lake
421 sediments and peat may be able to use this approach. New Zealand is highly suitable to develop a μ-
422 XRF method for geochemically fingerprinting rhyolitic tephra layers due to the rhyolitic eruptives
423 from several volcanoes and volcanic centres being significantly different in their geochemical
424 composition. On the other hand, many volcanic systems in the world have erupted tephras of similar
425 composition throughout their history (e.g., southern America, Iceland, Anatolia). These tephra may
426 not be identifiable by μ-XRF scanning. As μ-XRF data from sediment cores are routinely acquired in a
427 rapid, semi-automated and non-destructive manner, the μ-XRF based geochemical composition of
428 these tephra layers can easily be studied and compared for differences. An increase in XRF exposure
429 time and modern detector technology may provide crucial trace elemental data, which may highlight
430 differences between these tephra layers. Detailed scans and comparison to the volcanic source are
431 necessary on a regional scale if implementation of this μ-XRF based approach is sought outside of
432 New Zealand. In addition, studies need to be undertaken in sediment cores from marine and
433 minerogenic terrestrial depositional environments to widen the possible applicability of this
434 promising approach.

435 Established techniques such as EPMA and LA-ICP-MS acquire data from single grains/glass shards
436 whereas the μ-XRF scanner obtains data from the bulk of the tephra layer. In both techniques
437 measurements on 10 - 20 grains (EPMA, LA-ICP-MS) and over numerous downcore positions of the
438 tephra layer (μ-XRF) are obtained to capture subtle differences throughout a layer. Careful
439 comparison between EPMA-derived composition of glass shards and corresponding μ-XRF-based
440 composition of the bulk tephra layer are to be conducted in the future since we have now
441 demonstrated the general applicability of μ-XRF data to tephrochronology. Large compositional
442 heterogeneity in tephra layers due to pre- and syn-eruptive processes (Shane et al., 2008) rely on
443 EPMA or LA-ICP-MS measurements on separate grains or glass shards in EPMA or LA-ICP-MS. As a
444 result of the small step size of the μ-XRF core scanner, this technique may be employed to study

subtle differences in the chemical composition and grain size of tephra layers along the core axis, i.e., during its eruptive and/or depositional history.

Classical EPMA- and LA-ICP-MS-based chemical fingerprinting of tephra are supported by their stratigraphic order, physical properties such as thickness and colour, and independent ages to enable them to be correlated (Lowe et al., 2017). The same indicators must not be ignored in µ-XRF scanning based fingerprinting of tephra layers.

The speed of elemental scanning and wide range of elements detected in tephra layers makes the µ-XRF scanning approach a possible future tool for refining tephra correlation work in which traditional methods have failed to establish unambiguous correlations between given layers. This is partly the case with strong inhomogeneity in the 30+ basaltic tephra layers encountered in the AVF (Hopkins et al., 2015; 2017). Volcanic hazard assessment for Auckland city with >1.5 million inhabitants and infrastructure of national importance largely depends on correct tephra correlation and age estimates of tephra layers produced by eruptions from the AVF volcanoes.

Acknowledgements

We thank two anonymous reviewers for their helpful comments, which have strongly improved an earlier version of this manuscript. LP thanks the School of Environment, University of Auckland for supporting her participation in the Itrax Advanced Operator Training Course by Cox Analytical Systems in Stockholm, Sweden. LP expresses her gratitude to Cox Analytical Systems, in particular to Per Engström, for fundamental training and on-going support with data processing. LP acknowledges financial support from the University of Auckland Doctoral Scholarship and the Australian Institute for Nuclear Science and Engineering Post-Graduate Research Award.

Funding sources

Itrax scans at the University of Auckland have been funded by RSNZ Marsden Fund Contract UOA1415 and AINSE Ltd Award No. ALNGRA11064 (at ANSTO). Itrax scans at the Aberystwyth University were funded by Marsden contract UOA0415.

Conflict of Interest

The authors report no conflict of interest.

References

Aitchison, J., 1986. The statistical analysis of compositional data. Chapman and Hall, London; New York.

475 Augustinus, P., 2007. NZ-Maars: Extracting high resolution paleoclimate records from maar crater
476 lakes, Auckland, New Zealand. PAGES News 15, 18–20.

477 Augustinus, P., Reid, M., Andersson, S., Deng, Y., Horrocks, M., 2006. Biological and geochemical
478 record of anthropogenic impacts in recent sediments from Lake Pupuke, Auckland City, New
479 Zealand. Journal of Paleolimnology 35, 789–805. doi:10.1007/s10933-005-5306-8

480 Augustinus, P., Bleakley, N., Deng, Y., Shane, P., Cochran, U., 2008. Rapid change in early Holocene
481 environments inferred from Lake Pupuke, Auckland City, New Zealand. Journal of Quaternary
482 Science 23, 435–447. doi:10.1002/jqs.1153

483 Augustinus, P., D'Costa, D., Deng, Y., Hagg, J., Shane, P., 2011. A multi-proxy record of changing
484 environments from ca. 30000 to 9000 cal. a BP: Onepoto maar palaeolake, Auckland, New
485 Zealand. Journal of Quaternary Science 26, 389–401. doi:10.1002/jqs.1463

486 Balascio, N.L., Francus, P., Bradley, R.S., Schupack, B.B., Miller, G.H., Kvisvik, B.C., Bakke, J.,
487 Thordarson, T., 2015. Investigating the Use of Scanning X-Ray Fluorescence to Locate
488 Cryptotephra in Minerogenic Lacustrine Sediment: Experimental Results. In: Croudace, I.W.,
489 Rothwell, R.G. (Eds.), Micro-XRF Studies of Sediment Cores: Applications of a Non-Destructive
490 Tool for the Environmental Sciences. Springer Science+Business Media, Dordrecht, pp. 305–
491 324.

492 Cas, R.A.F., Wright, J. V., 1988. Volcanic Successions Modern and Ancient - A geological approach to
493 processes, products and successions, 1st ed. Chapman and Hall, London.

494 Cronin, S.J., Neall, V.E., Stewart, R.B., Palmer, A.S., 1996. A multiple-parameter approach to andesitic
495 tephra correlation, Ruapehu volcano, New Zealand. Journal of Volcanology and Geothermal
496 Research 72, 199–215. doi:10.1016/0377-0273(96)00008-X

497 Croudace, I.W., Rothwell, R.G., 2010. Micro-XRF sediment core scanners: important new tools for
498 the environmental and earth sciences. Spectroscopy Europe 22, 6–13.

499 Croudace, I.W., Rindby, A., Rothwell, R.G., 2006. ITRAX: description and evaluation of a new multi-
500 function X-ray core scanner. Geological Society, London, Special Publications 267, 51–63.
501 doi:10.1144/GSL.SP.2006.267.01.04

502 Cuven, S., Francus, P., Cremer, J.F., 2007. Protocoles d'utilisation et essais de calibration du scanner
503 de micro-fluorescence X de type "Itrax Core Scanner," Inrs-Ete.

504 Danišík, M., Shane, P., Schmitt, A.K., Hogg, A., Santos, G.M., Storm, S., Evans, N.J., Keith Fifield, L.,
505 Lindsay, J.M., 2012. Re-anchoring the late Pleistocene tephrochronology of New Zealand based

on concordant radiocarbon ages and combined 238U/ 230Th disequilibrium and (U-Th)/He zircon ages. Earth and Planetary Science Letters 349–350, 240–250. doi:10.1016/j.epsl.2012.06.041

Davies, S.J., Lamb, H.F., Roberts, S.J., 2015. Micro-XRF Core Scanning in Palaeolimnology: Recent Developments. In: Croudace, I.W., Rothwell, R.G. (Eds.), Micro-XRF Studies of Sediment Cores Applications of a Non-Destructive Tool for the Environmental Sciences. Springer, Dordrecht, p. 656.

Davies, S.M., Abbott, P.M., Pearce, N.J.G., Wastegård, S., Blockley, S.P.E., 2012. Integrating the INTIMATE records using tephrochronology: Rising to the challenge. Quaternary Science Reviews 36, 11–27. doi:10.1016/j.quascirev.2011.04.005

Dugmore, A.J., Newton, A.J., 2012. Isochrons and beyond: maximising the use of tephrochronology in geomorphology. Jökull 62, 39–52.

Feng, C., Wang, H., Lu, N., Chen, T., He, H., Lu, Y., Tu, X.M., 2014. Log-transformation and its implications for data analysis. Shanghai archives of psychiatry 26, 105–9. doi:10.3969/j.issn.1002-0829.2014.02.009

Hopkins, J.L., Millet, M.A., Timm, C., Wilson, C.J.N., Leonard, G.S., Palin, J.M., Neil, H., 2015. Tools and techniques for developing tephra stratigraphies in lake cores: A case study from the basaltic Auckland Volcanic Field, New Zealand. Quaternary Science Reviews 123, 58–75. doi:10.1016/j.quascirev.2015.06.014

Hopkins, J.L., Wilson, C.J.N., Millet, M.A., Leonard, G.S., Timm, C., McGee, L.E., Smith, I.E.M., Smith, E.G.C., 2017. Multi-criteria correlation of tephra deposits to source centres applied in the Auckland Volcanic Field, New Zealand. Bulletin of Volcanology 79. doi:10.1007/s00445-017-1131-y

Kylander, M.E., Lind, E.M., Wastegard, S., Lowemark, L., 2012. Recommendations for using XRF core scanning as a tool in tephrochronology. The Holocene 22, 371–375. doi:10.1177/0959683611423688

Lane, C.S., Lowe, D.J., Blockley, S.P.E., Suzuki, T., Smith, V.C., 2017. Advancing tephrochronology as a global dating tool: Applications in volcanology, archaeology, and palaeoclimatic research. Quaternary Geochronology 40, 1–7. doi:10.1016/j.quageo.2017.04.003

Leonard, G.S., Calvert, A.T., Hopkins, J.L., Wilson, C.J.N., Smid, E.R., Lindsay, J.M., Champion, D.E., 2017. High-precision 40Ar/39Ar dating of Quaternary basalts from Auckland Volcanic Field,

New Zealand, with implications for eruption rates and paleomagnetic correlations. Journal of Volcanology and Geothermal Research 343, 60–74. doi:10.1016/j.jvolgeores.2017.05.033

Lindsay, J., Leonard, G., Smid, E., Hayward, B., 2011. Age of the Auckland Volcanic Field: a review of existing data. New Zealand Journal of Geology and Geophysics 54, 379–401. doi:10.1080/00288306.2011.595805

Lowe, D.J., 2011. Tephrochronology and its application: A review. Quaternary Geochronology 6, 107–153. doi:10.1016/j.quageo.2010.08.003

Lowe, D.J., Shane, P.A.R., Alloway, B. V., Newnham, R.M., 2008. Fingerprints and age models for widespread New Zealand tephra marker beds erupted since 30,000 years ago: a framework for NZ-INTIMATE. Quaternary Science Reviews 27, 95–126. doi:10.1016/j.quascirev.2007.01.013

Lowe, D.J., Blaauw, M., Hogg, A.G., Newnham, R.M., 2013. Ages of 24 widespread tephras erupted since 30,000 years ago in New Zealand, with re-evaluation of the timing and palaeoclimatic implications of the Lateglacial cool episode recorded at Kaipo bog. Quaternary Science Reviews 74, 170–194. doi:10.1016/j.quascirev.2012.11.022

Lowe, D.J., Pearce, N.J.G., Jorgensen, M.A., Kuehn, S.C., Tryon, C.A., Hayward, C.L., 2017. Correlating tephras and cryptotephras using glass compositional analyses and numerical and statistical methods: Review and evaluation. Quaternary Science Reviews 175, 1–44. doi:10.1016/j.quascirev.2017.08.003

Löwemark, L., Chen, H.F., Yang, T.N., Kylander, M., Yu, E.F., Hsu, Y.W., Lee, T.Q., Song, S.R., Jarvis, S., 2011. Normalizing XRF-scanner data: A cautionary note on the interpretation of high-resolution records from organic-rich lakes. Journal of Asian Earth Sciences 40, 1250–1256. doi:10.1016/j.jseaes.2010.06.002

Martin-Puertas, C., Tjallingii, R., Bloemsma, M., Brauer, A., 2017. Varved sediment responses to early Holocene climate and environmental changes in Lake Meerfelder Maar (Germany) obtained from multivariate analyses of micro X-ray fluorescence core scanning data. Journal of Quaternary Science 32, 427–436. doi:10.1002/jqs.2935

Molloy, C., Shane, P., Augustinus, P., 2009. Eruption recurrence rates in a basaltic volcanic field based on tephralayers in maar sediments: Implications for hazards in the Auckland volcanic field. Bulletin of the Geological Society of America 121, 1666–1677. doi:10.1130/B26447.1

Newnham, R., Lowe, D.J., Gehrels, M., Augustinus, P., 2018. Two-step human–environmental impact history for northern New Zealand linked to late-Holocene climate change. Holocene.

568 doi:10.1177/0959683618761545

569 Nilsson, A., Muscheler, R., Snowball, I., Aldahan, A., Possnert, G., Augustinus, P., Atkin, D., Stephens,
570 T., 2011. Multi-proxy identification of the Laschamp geomagnetic field excursion in Lake
571 Pupuke, New Zealand. Earth and Planetary Science Letters 311, 155–164.
572 doi:10.1016/j.epsl.2011.08.050

573 Pearce, N.J.G., Denton, J.S., Perkins, W.T., Westgate, J.A., Alloway, B. V., 2007. Correlation and
574 characterisation of individual glass shards from tephra deposits using trace element laser
575 ablation ICP-MS analyses: current status and future potential. Journal of Quaternary Science
576 22, 721–736.

577 Pearce, N.J.G., Bendall, C.A., Westgate, J.A., 2008. Comment on "Some numerical considerations in
578 the geochemical analysis of distal microtephra" by A.M. Pollard, S.P.E. Blockley and C.S. Lane.
579 Applied Geochemistry 23, 1353–1364. doi:10.1016/j.apgeochem.2008.01.002

580 Pepper, A.C., Shulmeister, J., Nobes, D.C., Augustinus, P.A., 2004. Possible ENSO signals prior to the
581 Last Glacial Maximum, during the last deglaciation and the early Holocene, from New Zealand.
582 Geophysical Research Letters 31, 1–4. doi:10.1029/2004GL020236

583 Rothwell, R.G., Croudace, I.W., 2015. Twenty Years of XRF Core Scanning Marine Sediments: What
584 Do Geochemical Proxies Tell Us? In: Croudace, I.W., Rothwell, R.G. (Eds.), Micro-XRF Studies of
585 Sediment Cores Applications of a Non-Destructive Tool for the Environmental Sciences.
586 Springer, Dordrecht, p. 656.

587 Shane, P., 2000. Tephrochronology: A New Zealand case study, Earth Science Reviews.
588 doi:10.1016/S0012-8252(99)00058-6

589 Shane, P., 2005. Towards a comprehensive distal andesitic tephrostratigraphic framework for New
590 Zealand based on eruptions from Egmont volcano. Journal of Quaternary Science 20, 45–57.
591 doi:10.1002/jqs.897

592 Shane, P., Smith, I., 2000. Geochemical fingerprinting of basaltic tephra deposits in the Auckland
593 Volcanic Field. New Zealand Journal of Geology and Geophysics 43, 569–577.
594 doi:10.1080/00288306.2000.9514909

595 Shane, P., Nairn, I.A., Martin, S.B., Smith, V.C., 2008. Compositional heterogeneity in tephra deposits
596 resulting from the eruption of multiple magma bodies: Implications for tephrochronology.
597 Quaternary International 178, 44–53. doi:10.1016/j.quaint.2006.11.014

598 Shane, P.A.R., Froggatt, P.C., 1994. Discriminant Function Analysis of Glass Chemistry of New Zealand

599 and North American Tephra Deposits. Quaternary Research 41, 70–81.
600 doi:10.1006/qres.1994.1008

601 Smith, I.E.M., 1989. New Zealand Intraplate Volcanism: North Island. In: Johnson, R.W. (Ed.),
602 Intraplate Volcanism in Eastern Australia and New Zealand. Cambridge University Press,
603 Cambridge, UK, pp. 157–188.

604 Stephens, T., Atkin, D., Cochran, U., Augustinus, P., Reid, M., Lorrey, A., Shane, P., Street-Perrott, A.,
605 2012. A diatom-inferred record of reduced effective precipitation during the Last Glacial
606 Coldest Phase (28.8-18.0 cal kyr BP) and increasing Holocene seasonality at Lake Pupuke,
607 Auckland, New Zealand. Journal of Paleolimnology 48, 801–817. doi:10.1007/s10933-012-9645-
608 y

609 Stokes, S., Lowe, D.J., 1988. Discriminant function analysis of late Quaternary tephras from five
610 volcanoes in New Zealand using glass shard major element chemistry. Quaternary Research 30,
611 270–283. doi:10.1016/0033-5894(88)90003-8

612 Stokes, S., Lowe, D.J., Froggatt, P.C., 1992. Discriminant function analysis and correlation of Late
613 Quaternary rhyolitic tephra deposits from Taupo and Okataina volcanoes, New Zealand, using
614 glass shard major element composition. Quaternary International 13–14, 103–117.
615 doi:10.1016/1040-6182(92)90016-U

616 Striewski, B., Shulmeister, J., Augustinus, P.C., Soderholm, J., 2013. Late Holocene climate variability
617 from Lake Pupuke maar, Auckland, New Zealand. Quaternary Science Reviews 77, 46–54.
618 doi:10.1016/j.quascirev.2013.07.003

619 Thomson, J., Croudace, I.W., Rothwell, R.G., 2006. A geochemical application of the ITRAX scanner to
620 a sediment core containing eastern Mediterranean sapropel units. Geological Society, London,
621 Special Publications 267, 65–77. doi:10.1144/gsl.sp.2006.267.01.05

622 Wastegård, S., Veres, D., Kliem, P., Hahn, A., Ohlendorf, C., Zolitschka, B., 2013. Towards a late
623 Quaternary tephrochronological framework for the southernmost part of South America - the
624 Laguna Potrok Aike tephra record. Quaternary Science Reviews 71, 81–90.
625 doi:10.1016/j.quascirev.2012.10.019

626 Weltje, G.J., Tjallingii, R., 2008. Calibration of XRF core scanners for quantitative geochemical logging
627 of sediment cores: Theory and application. Earth and Planetary Science Letters 274, 423–438.
628 doi:10.1016/j.epsl.2008.07.054

629 Weltje, G.J., Bloemsma, M.R., Tjallingii, R., Heslop, D., Croudace, I.W., 2015. Prediction of

630 Geochemical Composition from XRF Core Scanner Data : A New Multivariate Approach
631 Including Automatic Selection of Calibration Samples and Quantification of Uncertainties. In:
632 Croudace, I.W., Rothwell, R.G. (Eds.), Micro-XRF Studies of Sediment Cores: Applications of a
633 Non-Destructive Tool for the Environmental Sciences. Springer Science+Business Media,
634 Dordrecht, pp. 507–534. doi:10.1007/978-94-017-9849-5

635 Winter, J.D., 2001. An Introduction to Igneous and Metamorphic Petrology. Prentice Hall Inc., Upper
636 Saddle River, New Jersey.

637 Zawalna-Geer, A., Lindsay, J.M., Davies, S., Augustinus, P., Davies, S., 2016. Extracting a primary
638 Holocene crytoptephra record from Pupuke maar sediments, Auckland, New Zealand. Journal
639 of Quaternary Science 31, 442–457. doi:10.1002/jqs.2866

640 Zelterman, D., 2015. Applied Multivariate Statistics with R. Springer, Heidelberg, New York,
641 Dordrecht, London. doi:10.1007/978-3-319-14093-3

642

643

Figure 1: Auckland Volcanic Field (left) with maar craters of this study highlighted in red and its position in New Zealand's North Island (right) in relation to the volcanic sources of the tephra layers found in the Auckland maars and wider New Zealand area: Tuhua (TUVC, peralkaline rhyolitic), Taupo (TVC, rhyolitic) and Okataina (OVC, rhyolitic), Egmont (Eg volcano, andesitic), Tongariro (TgVC, andesitic) and Auckland Volcanic Field (AVF, basaltic). VC: volcanic centre.

Figure 2: Variation of ten normalised elemental counts from µ-XRF core scanning across (A) six pre-KOT layers and (B) seven post-KOT layers alongside their optical core images. Note the contrast in µ-XRF data between enclosing sediment and rhyolite tephra layers.

Figure 3: Kernel density of normalised elemental counts of all 13 tephra layers analysed. Note how most elements approximate a log-normal distribution.

Figure 4: Kernel density of K_{norm} (up), Ca_{norm} (center), and Sr_{norm} (bottom) of all tephra µ-XRF core scanning data. Coloured lines differentiate between pre-identified tephra layers. Line pattern differentiates between Itrax lab locations of respective µ-XRF data. Note how, for example, the Tahuna tephra shows very different peaks depending on the scanning location whereas the Sr_{norm} peaks of the Rotoma tephra from UOA and UA almost overlap.

Figure 5: Principal component analysis of (A) log-ratio-transformed µ-XRF scanning results from the Onepoto core (pre-KOT) measured at ANSTO; (B) log-ratio-transformed µ-XRF scanning results from the Hopua core (post-KOT) measured at the University of Auckland; (C) and non-transformed µ-XRF scanning results as in B. Note how the log-transformed data plots in clusters with a larger spread of the datapoints than not transformed data. The log-transformed data also does not capture a cluster of the Tuhua tephra whereas not transformed data results in narrower clusters and captures clearly separated clusters for the Tuhua and Rotoma tephras.

Figure 6: Principal component analysis of (A) log-ratio-transformed µ-XRF scanning results from the rhyolitic tephra layers in the Onepoto core (pre-KOT) measured at ANSTO; (B) log-ratio-transformed µ-XRF scanning results from the rhyolitic tephra layers in the Hopua and Panmure cores (post-KOT) measured at UOA. Note how all thicker tephra layers with >50 data points (Rotoehu, Maketu, Rotorua, Rotoma, Tuhua) form clear clusters.

Figure 7: Linear discriminant analysis of (A) log-ratio-transformed µ-XRF scanning results from the rhyolitic tephra layers in the Onepoto core (pre-KOT) measured at ANSTO; (B) log-ratio-transformed µ-XRF scanning results from the rhyolitic tephra layers in the Hopua and Panmure cores (post-KOT) measured at the University of Auckland. Note that LD2 enables discrimination between the source

volcanic centres (TVC and OVC) in (A) and LD1 separates TU vs. TVC+OVC, whilst LD3 separates TVC vs. OVC+MI in (B). Black arrows mark the direction of relative enrichment of elements listed.

Figure 8: Bivariate scatter plots of six elemental ratios of (A) log-transformed µ-XRF scanning results from the rhyolitic tephra layers in the Onepoto core (pre-KOT) measured at ANSTO; (B) log-transformed µ-XRF scanning results from the rhyolitic tephra layers in the Hopua and Panmure cores (post-KOT) measured at the University of Auckland. Note how most plots allow for clear separation of the thicker tephra layers (Okaia, Maketu, Rotoehu in (A); Tuhua, Rotoma, Opepe and Rotorua tephra in (B)).

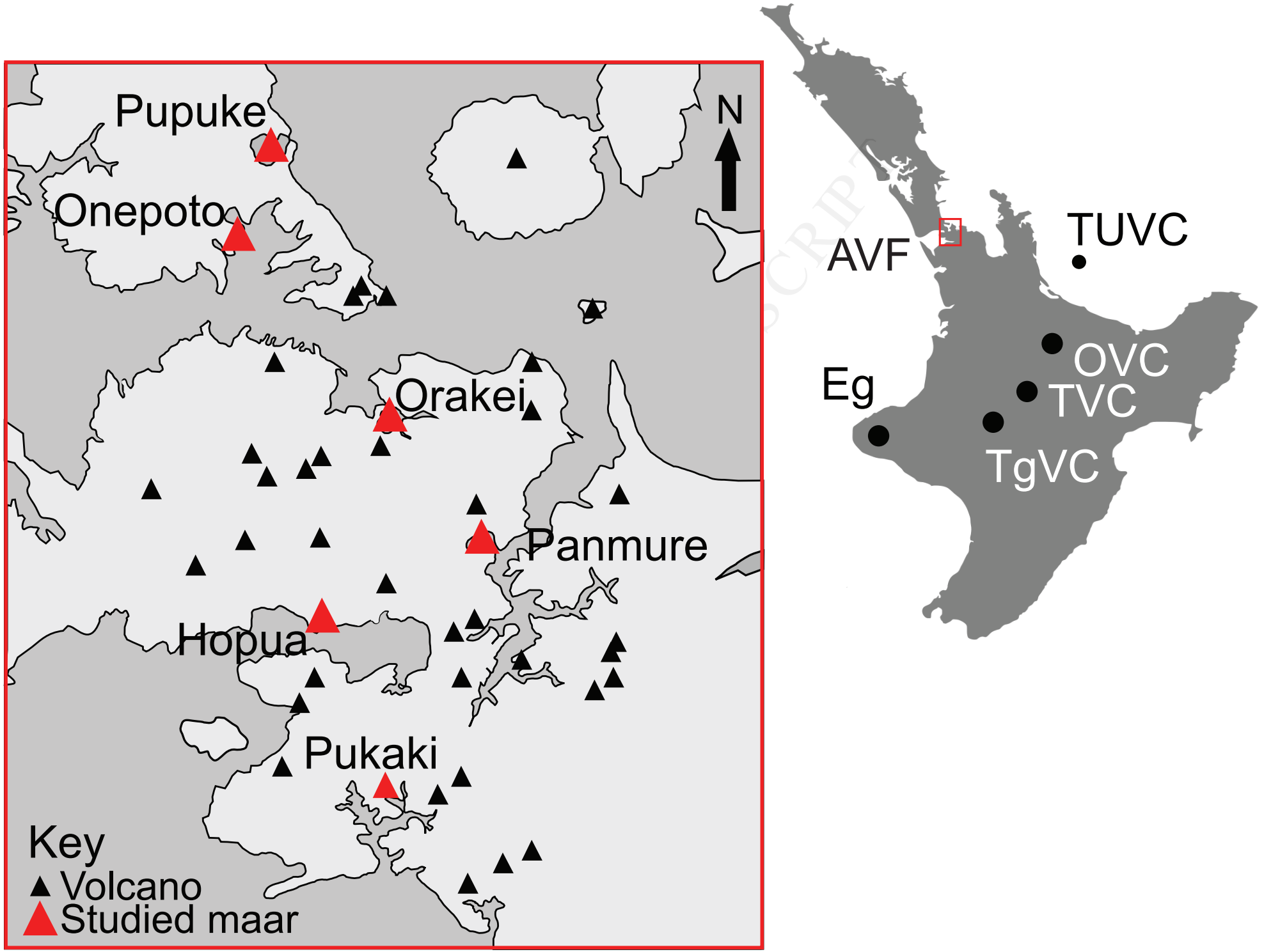

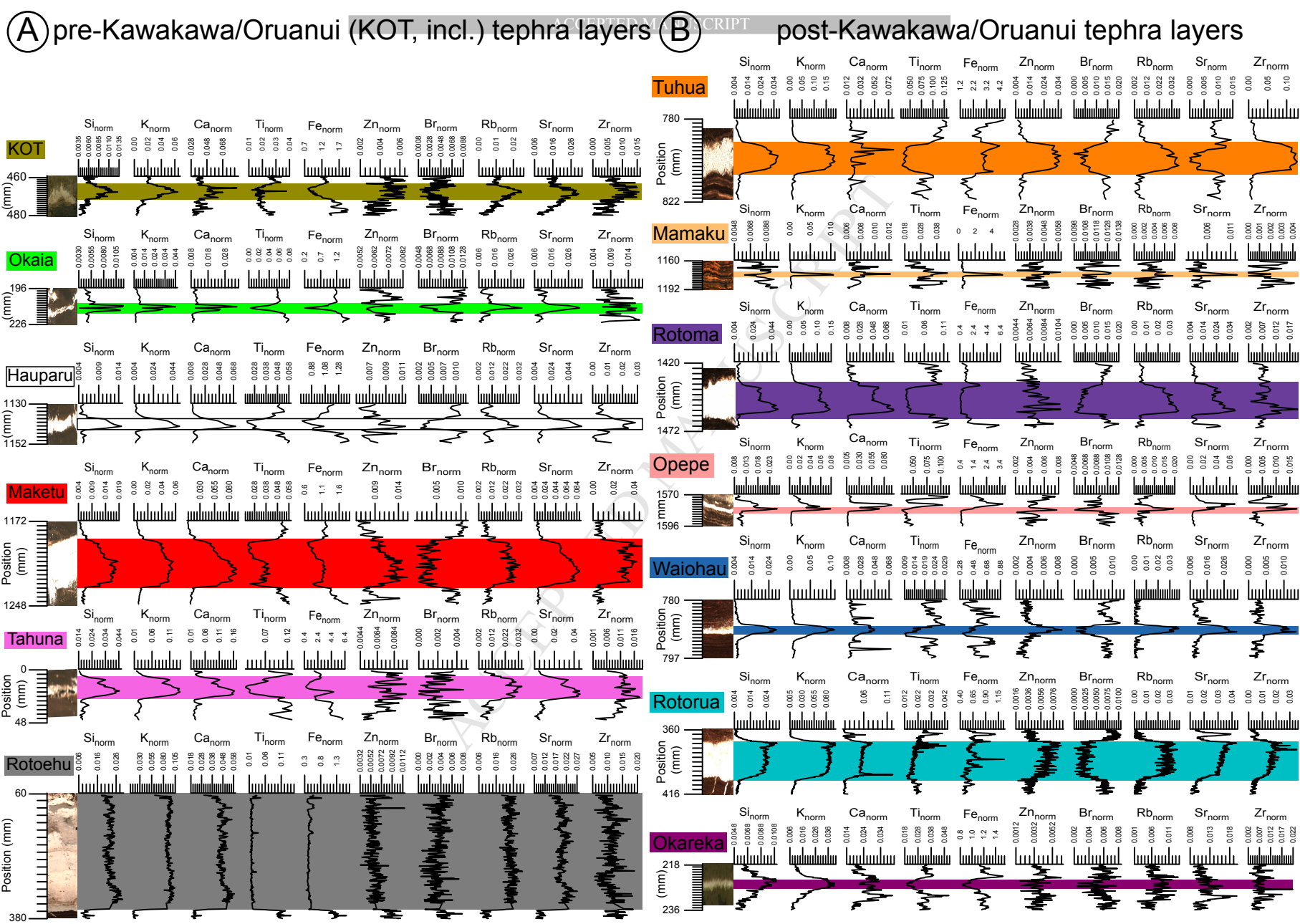

Kernel density plots of elements X_{norm} and inc/coh scattering ratio (all 13 tephra layers, all measurements, not transformed)

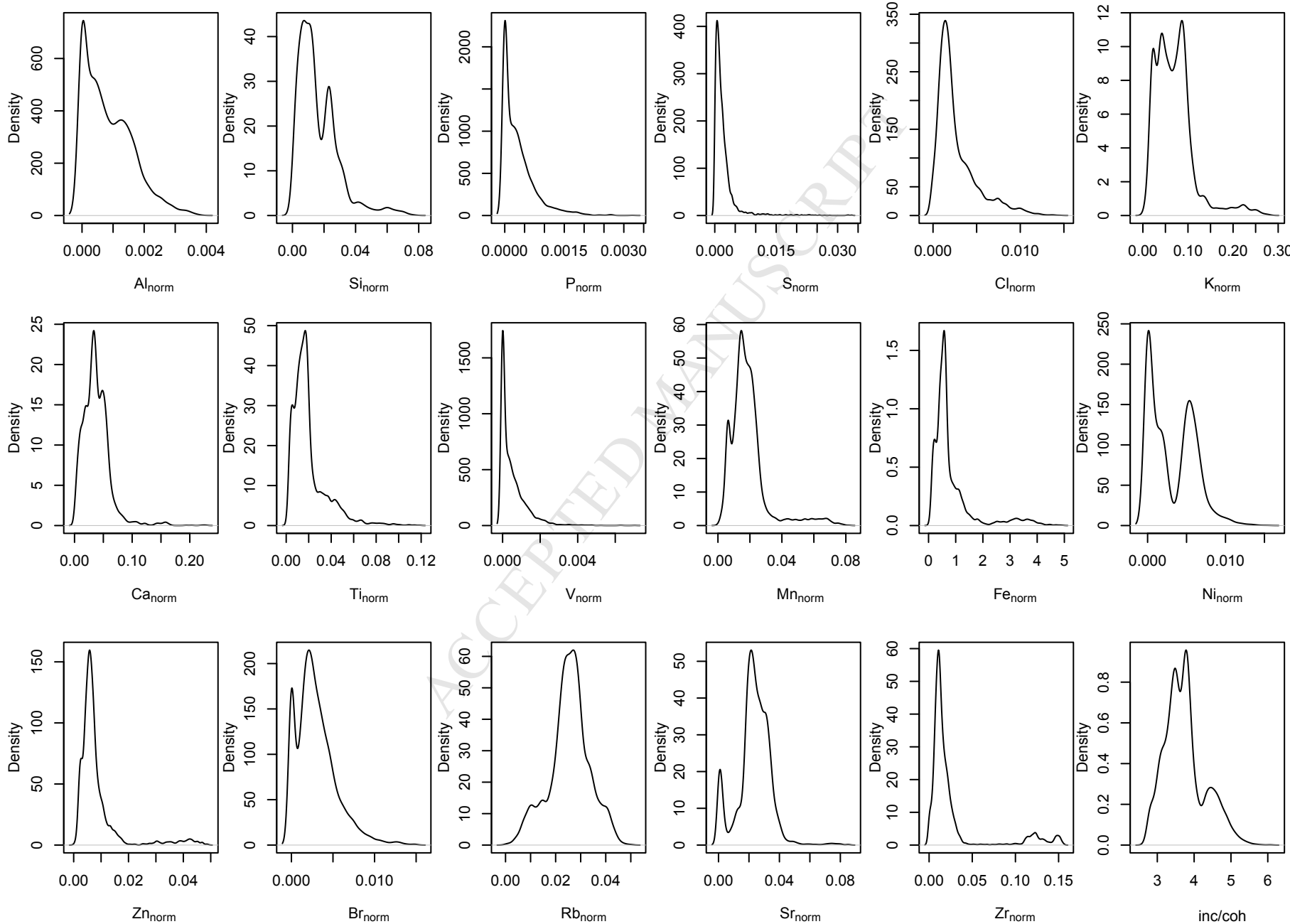

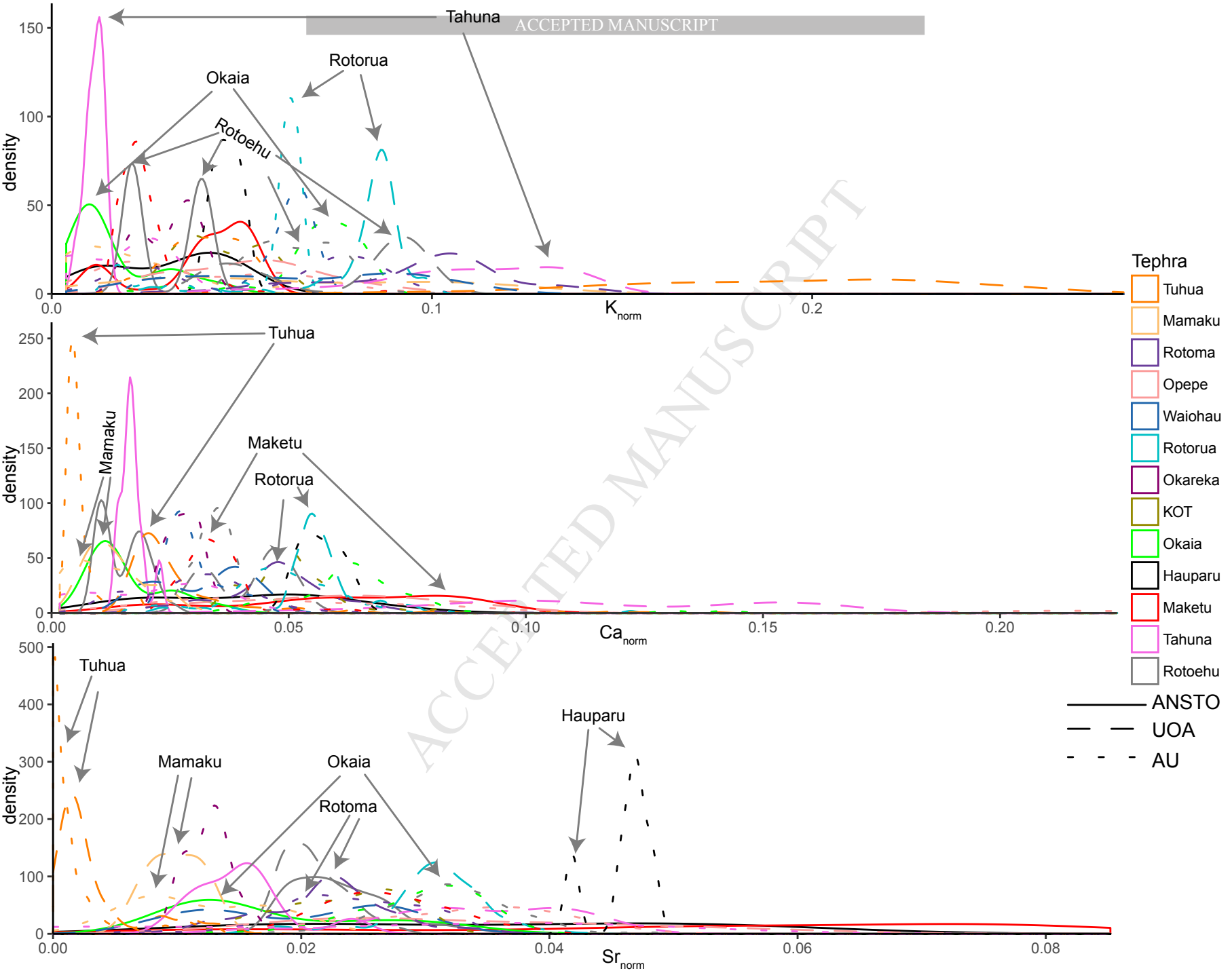

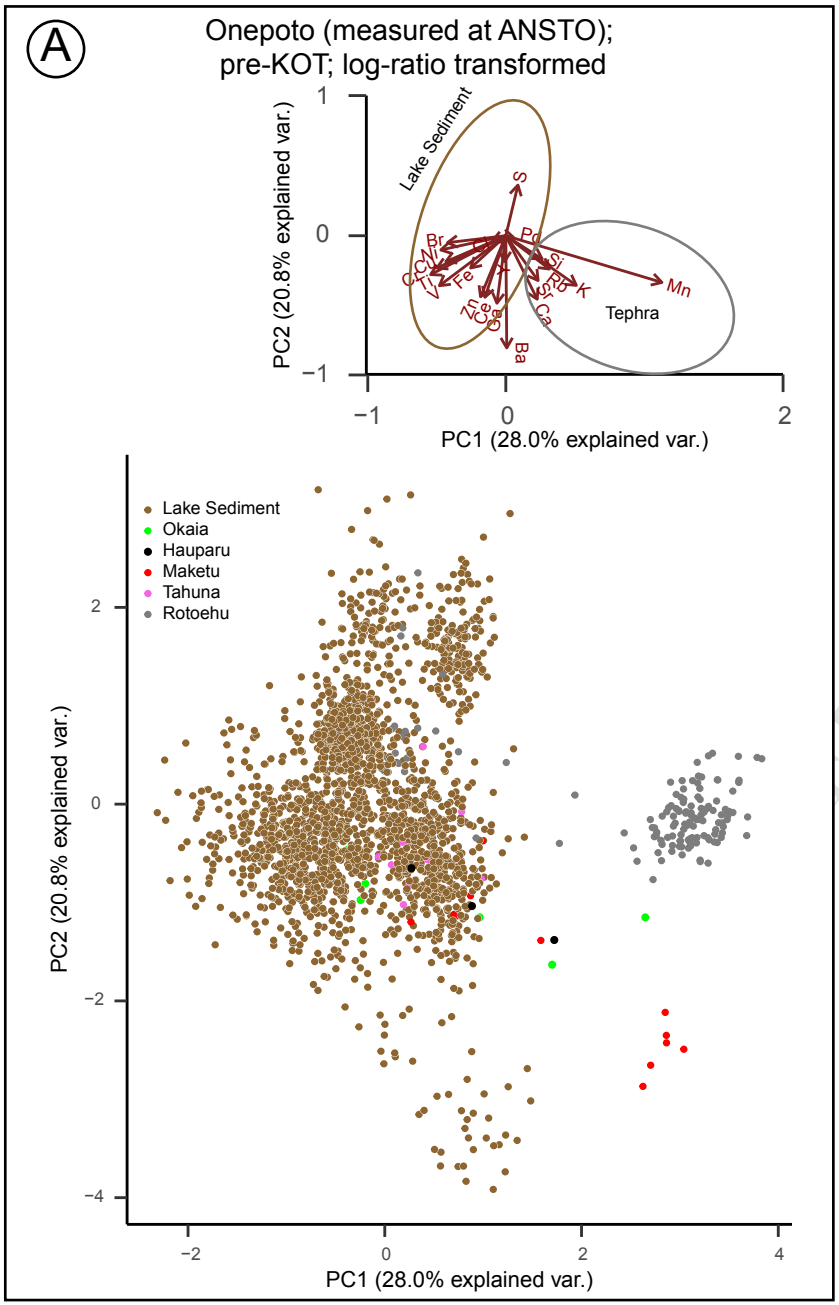

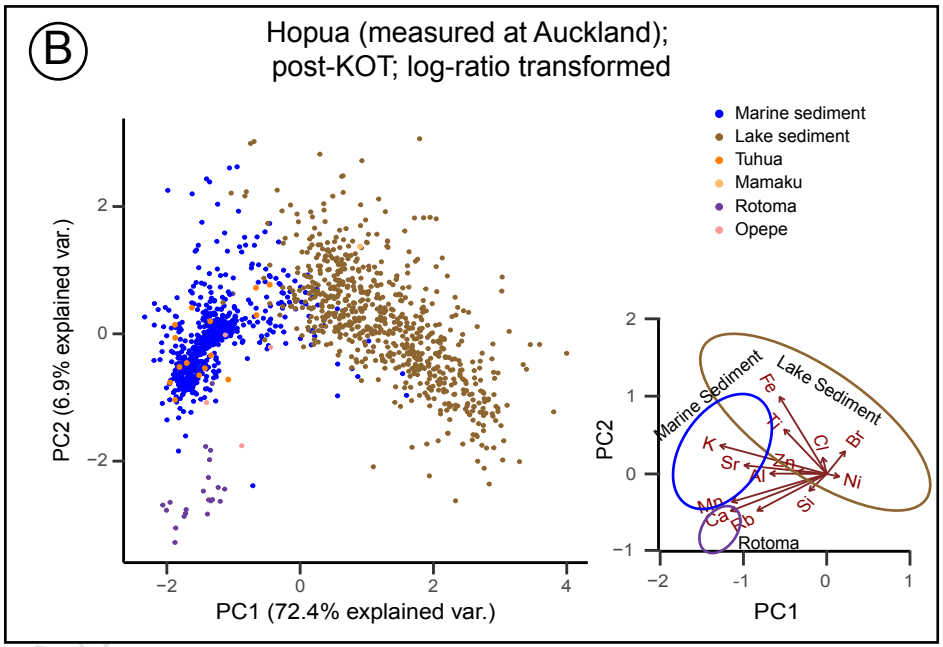

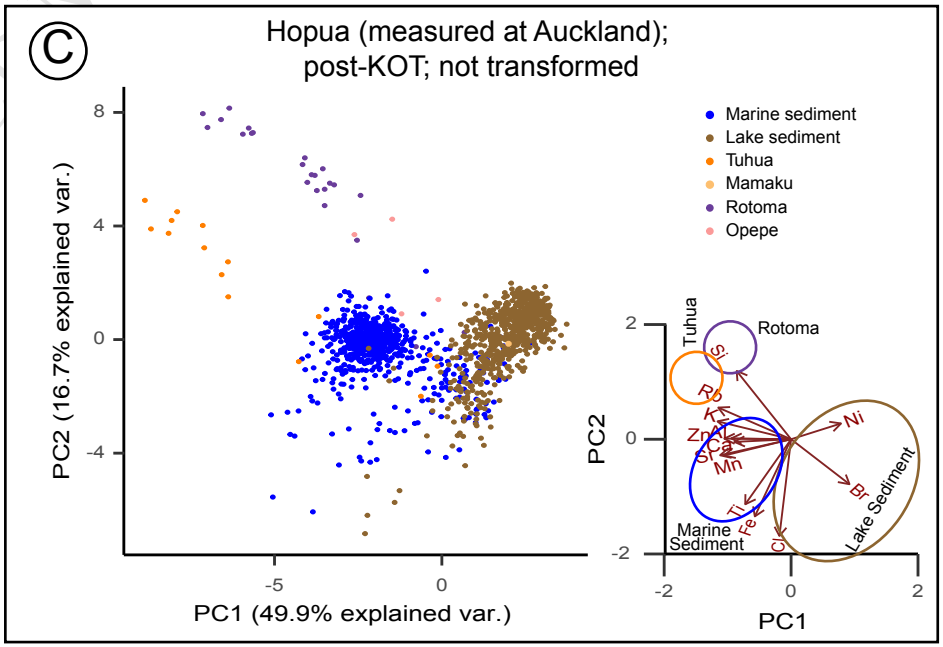

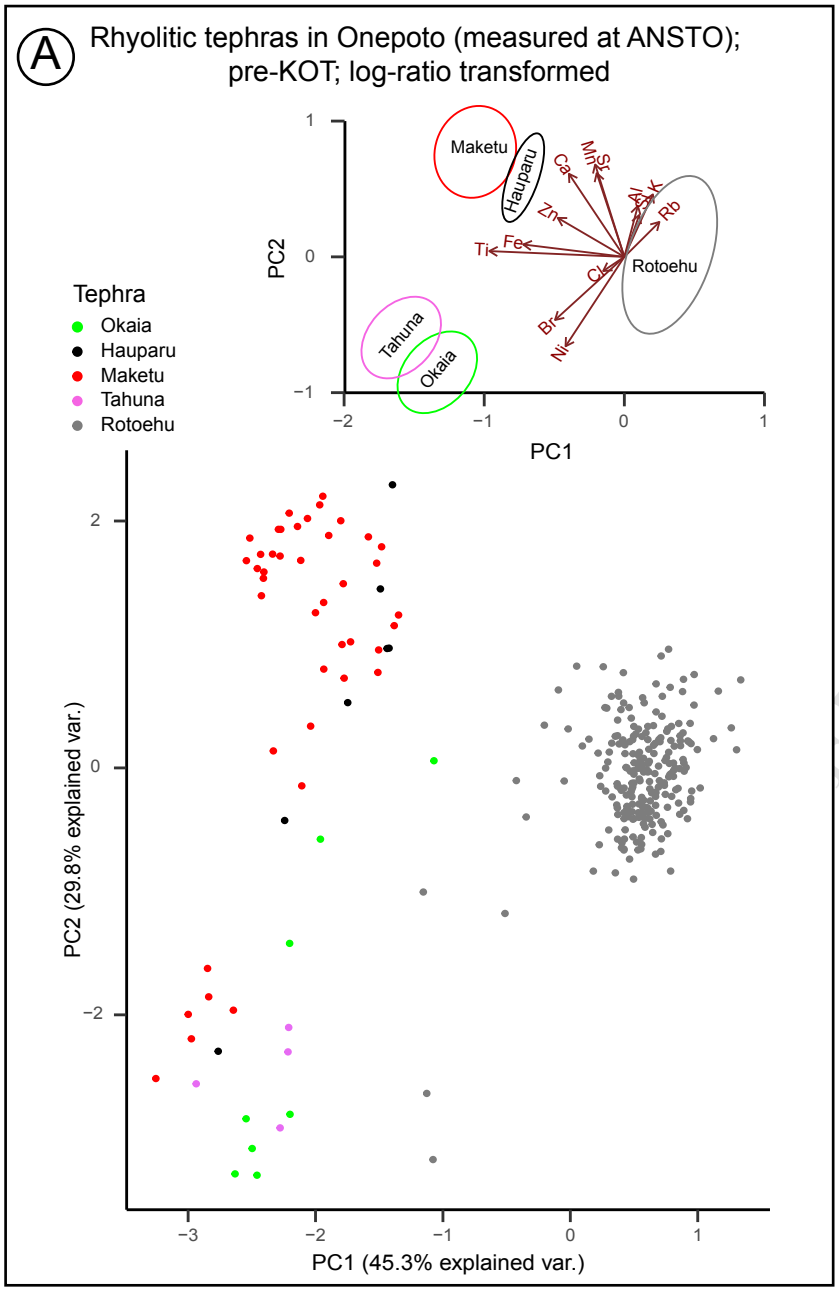

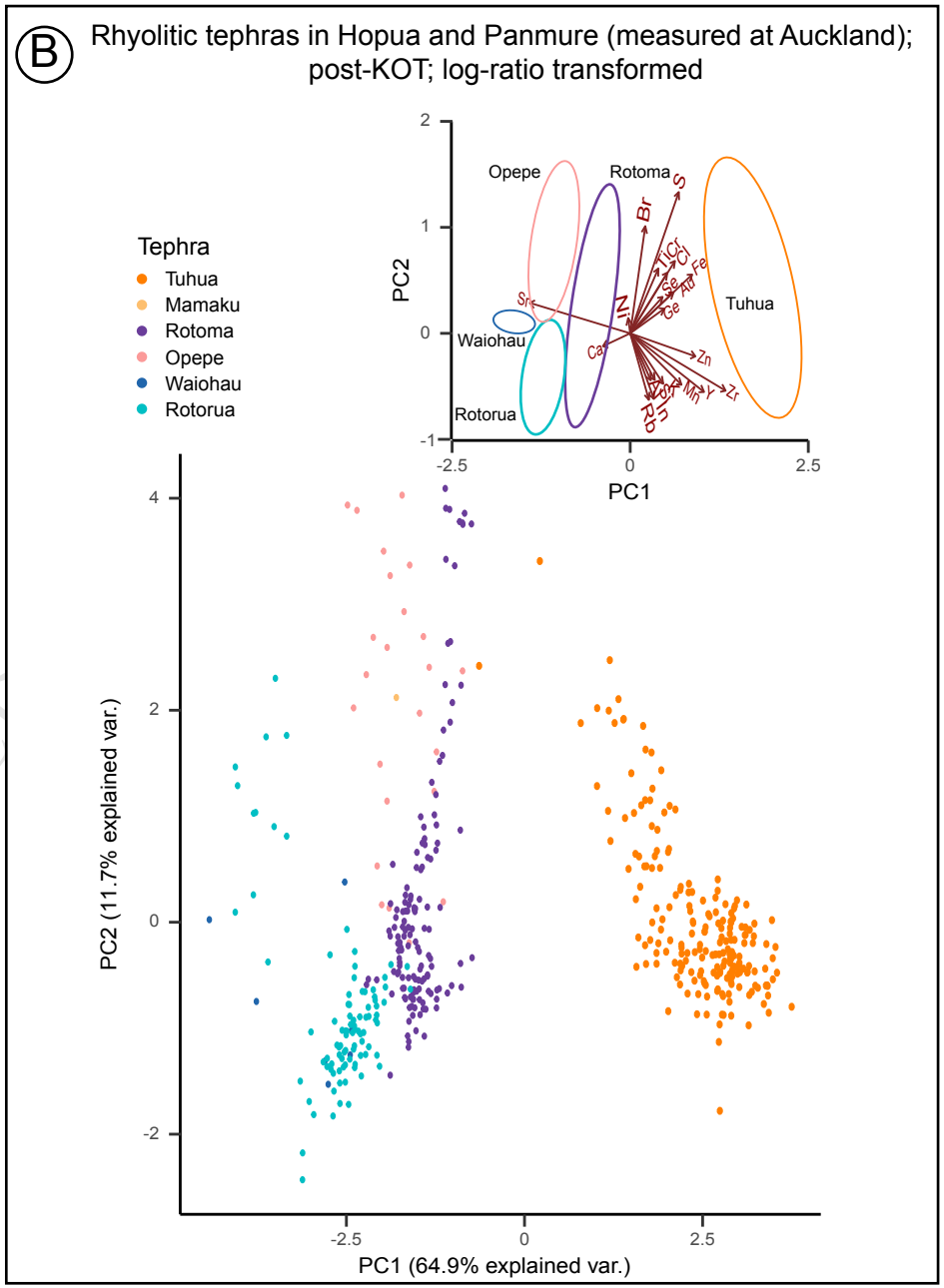

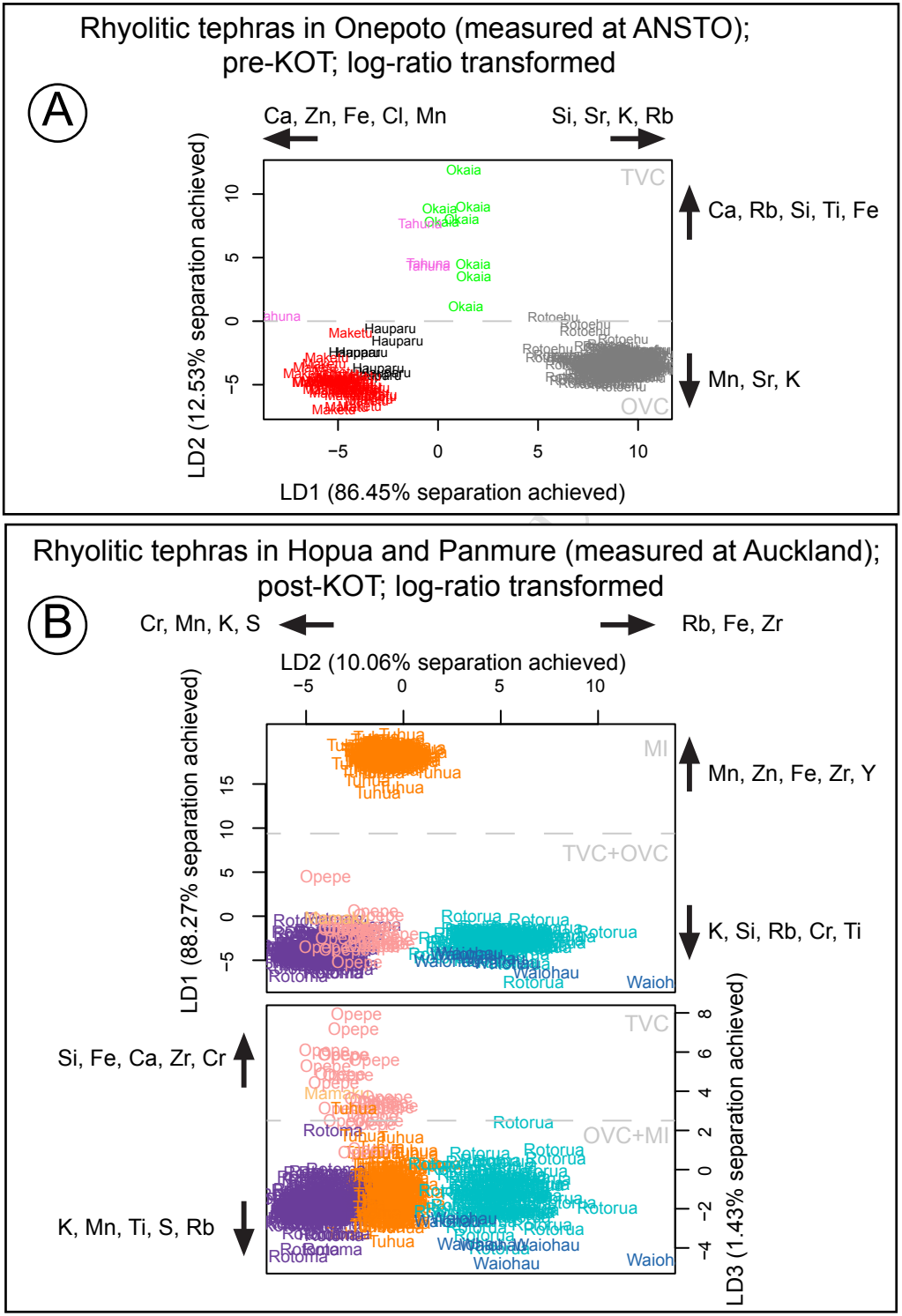
Rhyolitic tephras in Onepoto (measured at ANSTO); pre-KOT; log-ratio transformed
A
Ca, Zn, Fe, Cl, Mn
Si, Sr, K, Rb
LD2 (12.53% separation achieved)
LD1 (86.45% separation achieved)
TVC
OVC
Ca, Rb, Si, Ti, Fe
Mn, Sr, K
Okaia
Tahuna
Hauparu
Maketu
Rotoehu
Rhyolitic tephras in Hopua and Panmure (measured at Auckland); post-KOT; log-ratio transformed
B
Cr, Mn, K, S
Rb, Fe, Zr
LD2 (10.06% separation achieved)
LD1 (88.27% separation achieved)
MI
TVC+OVC
Mn, Zn, Fe, Zr, Y
K, Si, Rb, Cr, Ti
Tuhua
Opepe
Rotorua
Waiohau
Si, Fe, Ca, Zr, Cr
K, Mn, Ti, S, Rb
TVC
OVC+MI
LD3 (1.43% separation achieved)

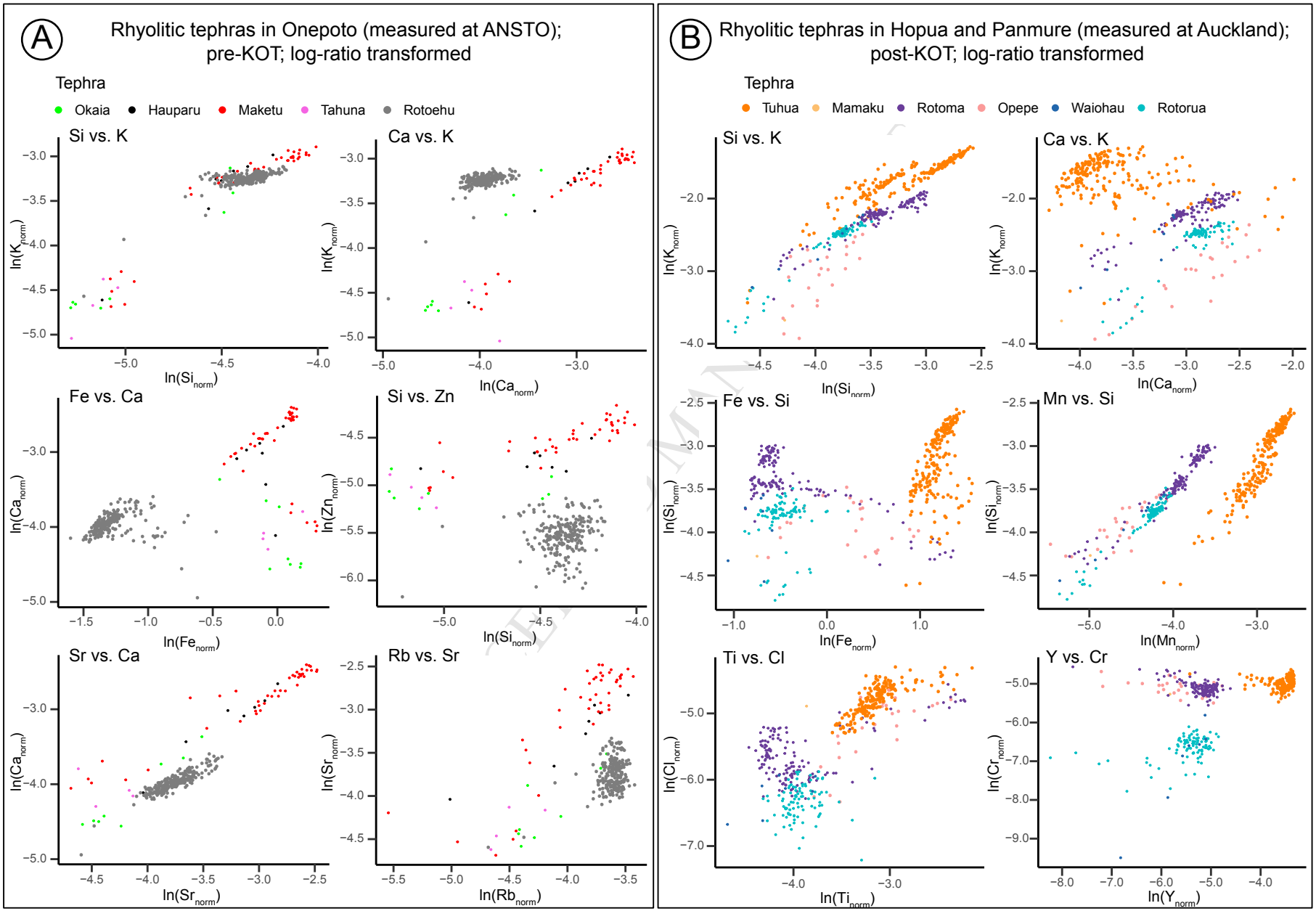
A
Rhyolitic tephras in Onepoto (measured at ANSTO); pre-KOT; log-ratio transformed
Tephra
Okaia
Hauparu
Maketu
Tahuna
Rotoehu
Si vs. K
Ca vs. K
Fe vs. Ca
Si vs. Zn
Sr vs. Ca
Rb vs. Sr
B
Rhyolitic tephras in Hopua and Panmure (measured at Auckland); post-KOT; log-ratio transformed
Tephra
Tuhua
Mamaku
Rotoma
Opepe
Waiohau
Rotorua
Si vs. K
Ca vs. K
Fe vs. Si
Mn vs. Si
Ti vs. Cl
Y vs. Cr